ACS APPLIED MATERIALS & INTERFACES
Research Article
www.acsami.org

Enhanced Current Transport and Injection in Thin-Film Gallium-Nitride Light-Emitting Diodes by Laser-Based Doping

Su Jin Kim,[†] Kyeong Heon Kim,[†] Ho Young Chung,[†] Hee Woong Shin,[†] Byeong Ryong Lee,[†] Tak Jeong,[‡] Hyung Jo Park,[‡] and Tae Geun Kim*,[†]

[†]School of Electrical Engineering, Korea University, Anam-dong, Seongbuk-gu, Seoul 136-701, Republic of Korea

[‡]LED Device Research Center, Korea Photonics Technology Institute, Gwangju 500-779, Republic of Korea

Supporting Information

ABSTRACT: This paper reports improvements in the electrical and optical properties of blue-emission gallium nitride (GaN)-based thin-film light-emitting diodes (TFLEDs) after laser-based Si doping (LBSD) of a nitrogen-face n-GaN (denoted as hereafter n-GaN) layer. Experimental results show that the light-output powers of the flat- and rough-surface TFLEDs after LBSD are 52.1 and 11.35% higher than those before LBSD, respectively, at a current of 350 mA, while the corresponding operating voltages are decreased by 0.22 and 0.28 V for the flat- and rough-surface TFLEDs after LBSD, respectively. The reduced operating voltage after LBSD of the top n-GaN layer may result from the remarkably decreased specific contact resistance at the metal/n-GaN interface and the low series resistance of the TFLED device. The LBSD of n-GaN increases the number of nitrogen vacancies, and Si substitutes for Ga (Si_{Ga}) at the metal/n-GaN interface to produce highly Si-doped regions in n-GaN, leading to a decrease in the Schottky barrier height and width. As a result, the specific contact resistances are significantly decreased to 1.56×10^{-5} and 2.86×10^{-5} Ω cm^2 for the flat- and rough-surface samples after LBSD, respectively. On the other hand, the increased light-output power after LBSD can be explained by the uniform current spreading, efficient current injection, and enhanced light scattering resulting from the low contact resistivity, low lateral current resistance, and additional textured surface, respectively. Furthermore, LBSD did not degrade the electrical properties of the TFLEDs owing to low reverse leakage currents. The results indicate that our approach could potentially enable high-efficiency and high-power capabilities for optoelectronic devices.

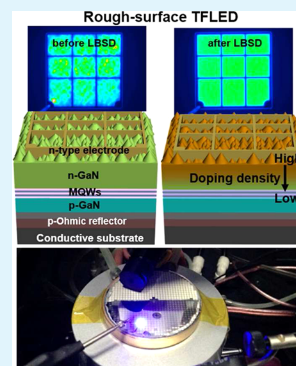

KEYWORDS: *laser, Si doping, GaN, thin film, LEDs*

1. INTRODUCTION

Gallium nitride (GaN)-based materials having direct band gap transitions are important and essential for light-emitting diodes (LEDs) operating in the ultraviolet (UV) to visible spectrum.[1] Recently, considerable progress in the external quantum efficiency of GaN-based LEDs has been achieved owing to advantages in epitaxial growth and chip fabrication; therefore, they have been widely applied in various areas such as full-color displays, automotive lighting, backlight units for liquid-crystal displays, and interior/exterior lighting.[2,3] In particular, GaN-based thin-film LEDs (TFLEDs) have been suggested as a solution for next-generation solid-state light sources because of their superior performance such as a larger emitting area, better current distribution, superb light extraction, and superior heat dissipation.[4−7] However, despite these advantages, the light-output power and efficiency of TFLEDs are still not sufficiently high; thus, further improvements should be achieved for their practical use in general lighting.

One of the important issues for improving the overall efficiency and device performance of TFLEDs is to obtain a low contact resistance and efficient current injection/distribution, thereby achieving a low operating voltage and high-power output. For TFLEDs, an n-type ohmic contact is formed on an n-GaN layer with a (000−1) N-face surface orientation because the sapphire substrates are detached from the LED epilayers using a laser lift-off (LLO) process. Therefore, it is generally difficult to obtain a low specific contact resistance less than $\sim 1 \times 10^{-4}$ Ω cm^2 for an n-GaN ohmic contact, and nonohmic behavior is observed after thermal annealing at temperatures greater than 300 °C.[8] These issues are attributed to the formation of complex surface states including impurities and defects[9] as well as electrical compensation effects due to the spontaneous polarization toward the [000−1] direction[10] of the n-GaN surface in TFLEDs. Because a high contact resistance hampers effective current injection during LED operation, the output power and external quantum efficiency are degraded in this ohmic-contact scheme.[11,12]

Another critical issue for TFLEDs is the nonuniform current distribution and injection over entire n-GaN layers, leading to localized light emission in the proximity of the n-type electrodes. This is because the large chip size and large lateral resistance due to the thin n-GaN layers and top-down electrode

Received: May 21, 2014
Accepted: September 12, 2014
Published: September 12, 2014

ACS Publications © 2014 American Chemical Society

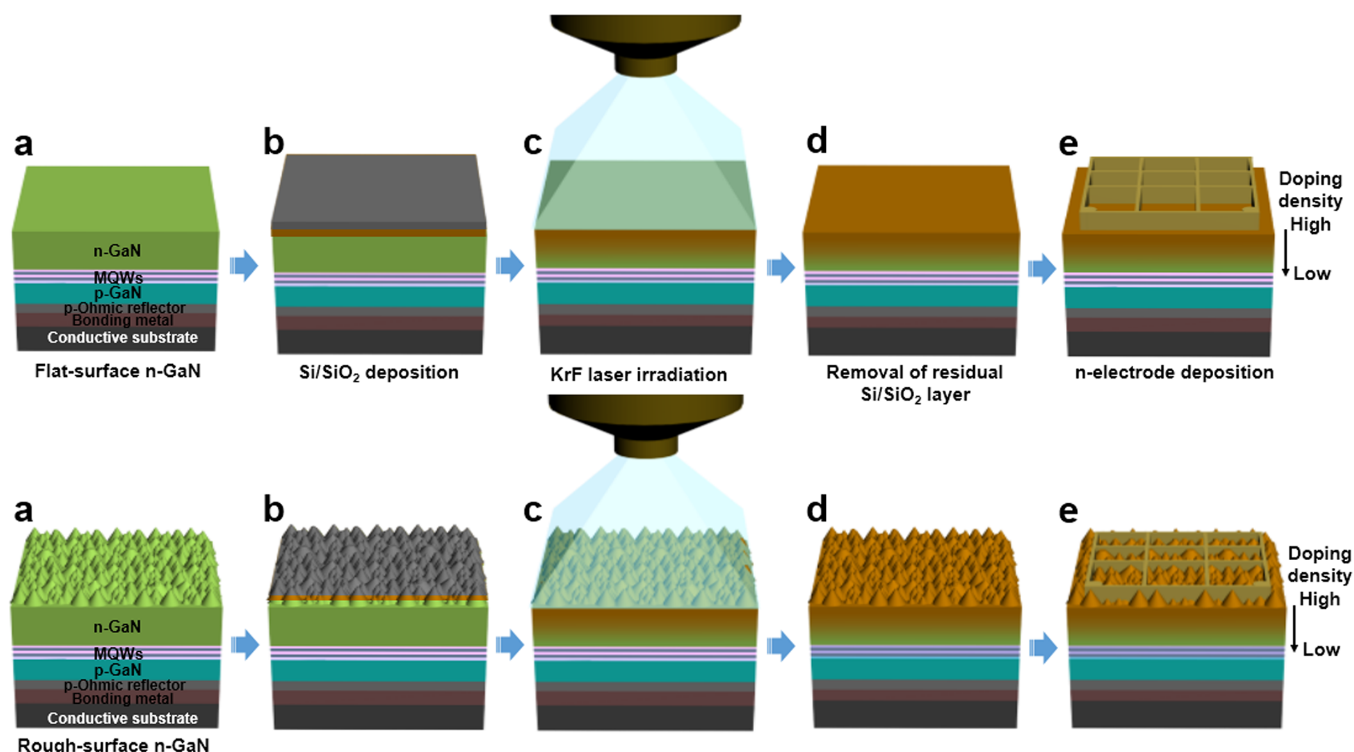

Figure 1. Schematic representation of the LBSD process flow for the fabricated TFLEDs: (a) flat- and rough-surface TFLEDs, (b) deposition of the Si film and SiO_2 capping layer, (c) schematic of KrF laser irradiation of the flat- and rough-surface TFLEDs, (d) removal of the residual Si film and SiO_2 layer, and (e) n-electrode deposition.

scheme in TFLEDs increase the current density beneath the n-type electrodes, eventually deteriorating the device reliability, electrical properties, and light-output power of the TFLEDs. Although these problems can be alleviated to some extent by optimizing the design of the n-type electrodes, such as a branch- or finger-shaped design,[13] some losses in light emission are unavoidable because the photons generated in the multiquantum wells (MQWs) are blocked by the opaque n-type metal electrodes.

To solve these problems, some groups used a transparent conductive layer (TCL) such as indium tin oxide (ITO),[14] indium zinc oxide (IZO),[15] and graphene[16] on the n-GaN layers of the TFLEDs to improve the current spreading efficiency. However, the TCL methods have not perfectly provided large enhancements in both the light-output power and operating voltage because of the trade-off between the optical transmittance and the electrical conductivity. For example, light extraction from the top surface decreases owing to optical losses (low transmittance) via ITO and IZO TCLs, leading to a reduction in the light-output power. For a graphene TCL, electrical degradation (or a high operating voltage) is observed owing to the high sheet and contact resistances as a result of the large work-function difference between graphene and the n-GaN layer. Therefore, it is necessary to find a way to achieve both a low-resistance nonalloyed ohmic contact and effective current injection/distribution properties to develop high-efficiency and high-power TFLEDs.

In this paper, a laser-based Si doping (LBSD) method is employed for the n-GaN layers of TFLEDs to obtain not only low-resistance nonalloyed ohmic contacts on n-GaN but also a uniform current distribution and highly efficient current injection in TFLEDs, thereby reducing the operating voltage and increasing the light-output power. Further, the electrical and optical properties of flat- and rough-surface TFLEDs before LBSD are investigated and compared with those of flat- and rough-surface TFLEDs after LBSD.

2. EXPERIMENTAL METHODS

In this experiment, two different TFLED samples with flat and rough n-GaN surface were prepared for comparison. To fabricate the GaN-based TFLED samples, metalorganic chemical vapor deposition (MOCVD) was used to grow the GaN-based LED epitaxial layers (epilayers). Prior to the growth of the GaN buffer layer, a low-temperature GaN nucleation layer was first grown on double-side-polished c-plane (0001) 2-in.-diameter sapphire wafers. Then, a 2-μm-thick unintentionally doped GaN buffer layer, a 3 μm thick layer of n-GaN doped with Si (average n-type doping concentration of 5×10^{18} cm^{-3}), an active region with five pairs of InGaN/GaN MQWs, a 20 nm-thick p-type AlGaN electron-blocking layer, and a 200 nm-thick layer of p-type GaN doped with Mg (average p-type doping concentration of 1×10^{18} cm^{-3}) were sequentially deposited. After the final growth of the p-type GaN-terminated LED epilayers, a silicon oxide (SiO_2) current blocking layer (CBL) was formed on the LED epilayers using a combination of photolithography and wet etching with a buffered oxide etchant (BOE) to fabricate the TFLED chip. A p-type ohmic reflector with a Ni/Ag-based contact scheme was then deposited onto the LED epilayers, followed by annealing at 500 °C for 1 min in a nitrogen atmosphere to obtain p-type ohmic properties. A AuSn-based metallic layer was deposited onto the LED epilayers prior to the wafer-bonding process, and the 2-in. diameter wafer with the LED epilayers was then bonded to a 2-in.-diameter molybdenum metal substrate by thermal compression at 300 °C for 20 min to support the LED epilayers during a laser lift-off (LLO) process. Next, the sapphire substrate was separated from the LED epilayers by LLO with a QMC Inc., ELMS 1000 KrF pulsed excimer laser system (248 nm). After the LLO process, the exposed undoped GaN surface of the n-side-up wafer-level sample was etched with a HCl solution [HCl/deionized (DI) water =1:1] for 3 min to remove residual Ga droplets. Then, the

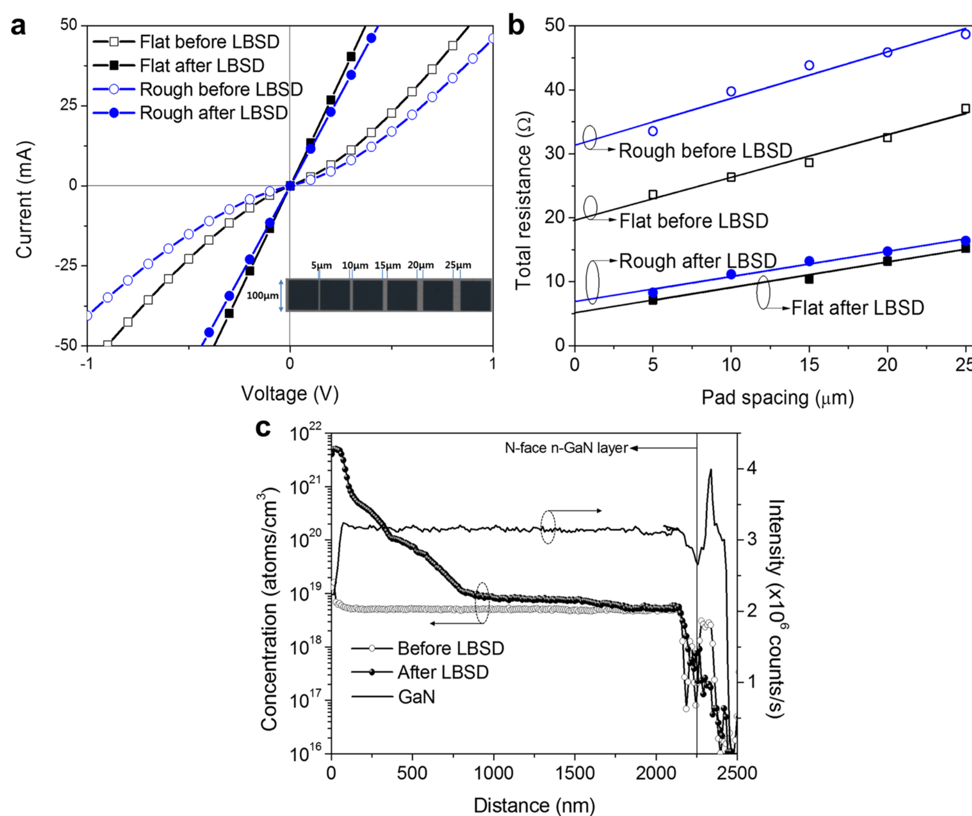

Figure 2. (a) Typical current−voltage ($I-V$) characteristics and (b) the total resistance as a function of the pad gap spacing of Ti/Al-based metal contacts on flat- and rough-surface n-GaN before and after LBSD. The inset images show that the TLM pattern structures consist of a contact-pad width of 100 μm and gaps between the contact pads of 5, 10, 15, 20, and 25 μm. $I-V$ data were measured from the two contact pads with a gap distance of 5 μm. (c) Doping depth profile of Si atoms measured from n-GaN before and after LBSD.

undoped GaN layer was etched using inductively coupled plasma (ICP) reactive-ion etching (RIE) to expose the flat n-GaN surface. Photolithography and ICP-RIE processes were used to define the chip-to-chip electrical isolation, and a SiO_2 passivation layer was deposited onto the isolation region. In addition, to fabricate the TFLEDs with rough n-GaN surface, we performed n-GaN surface roughening using 6-mol potassium hydroxide (KOH)-based wet etching at 70 °C for 15 min. Finally, Ti/Al/Ni/Au was deposited onto the n-GaN surface as an n-type electrode by electron-beam evaporation. The fabricated TFLED chip size including the isolated-mesa region between chips is approximately 1.4 mm × 1.4 mm. Further details of the flat and rough n-GaN surface images as well as schematic drawings of the TFLED chip fabrication process are presented in the Supporting Information, Figure S1.

Figure 1 shows a schematic illustration for a key step process of LBSD. Prior to n-type metal deposition, 100 nm-thick Si and 100 nm-thick SiO_2 films were sequentially deposited on the flat and rough n-GaN surfaces of TFLEDs using radio frequency magnetron sputtering, which were loaded onto the *x-y-z* axis moveable stage by controlling the laser irradiation system (see the Supporting Information, Figure S2). The Si and SiO_2 films were used as dopant and capping layers, respectively, to prevent severe damage to the n-GaN layer of the TFLEDs. Using the KrF pulsed laser with a wavelength of 248 nm, five pulses of the laser beam with a laser energy density of 600 mJ/cm^2, a repetition rate of 50 Hz, and a square-shaped beam size of 1.4 mm × 1.4 mm were used to irradiate the n-GaN surface. It is generally known that laser irradiation at 600 mJ/cm^2 could increase the n-GaN surface temperature up to approximately 900−1000 °C, which is a sufficiently high temperature for Si diffusion and activation in GaN.[17,18] Thus, the absorption of the laser energy during laser scanning causes an increase in the temperature in the Si and n-GaN layers, and the energetic Si atoms can then diffuse into the lattice of the n-GaN layer, resulting in the formation of a highly doped layer. After finishing LBSD, the residual SiO_2 and Si layers were sequentially removed by dipping in the BOE and a HNO_3/DI water/HF solution at a ratio of 100:140:3 by volume, respectively. To compare and analyze the performance without a difference in epitaxial quality, four types of TFLEDs with different n-GaN layer structures were fabricated using the same epiwafer: the flat-surface TFLEDs before and after LBSD (denoted hereafter as the flat before LBSD sample and the flat after LBSD sample, respectively) and the rough-surface TFLEDs before and after LBSD (denoted hereafter as the rough before LBSD sample and the rough after LBSD sample, respectively).

To determine the specific contact resistance, we used a linear transmission-line method (TLM), where the pattern structures are shown in the inset of Figure 2a. The Ti (30 nm)/Al (200 nm) metal stacks with the TLM patterns were defined by photolithography, and a metal lift-off process was then carried out. Before contact metal deposition, the n-GaN surface was immersed in a BOE solution for 1 min and was rinsed using DI water. After that, the current−voltage (I−V) characteristics of the TLM contacts were measured utilizing a Keithley 4200 semiconductor parameter analyzer. Secondary ion-mass spectrometry (SIMS) and X-ray photoelectron spectroscopy (XPS, X-tool, ULVAC-PHI) were used to investigate the doping concentration and surface states of the n-GaN layer. The electrical and optical characteristics were measured at the wafer level by using a wafer-level LED probe station (OPI-150, WithLight CO., Ltd.). It must be noted that the average values measured for 20 LED chips randomly selected from each type of LED sample were used in this study. In addition, the surface morphology was observed by atomic force microscopy (AFM, XE-100 Park Systems). The light distribution images of the TFLED chips were taken by a photoemission microscope.

3. RESULTS AND DISCUSSION

Prior to the fabrication of the TFLEDs with different types of n-GaN layers, we first systematically evaluated the influence of

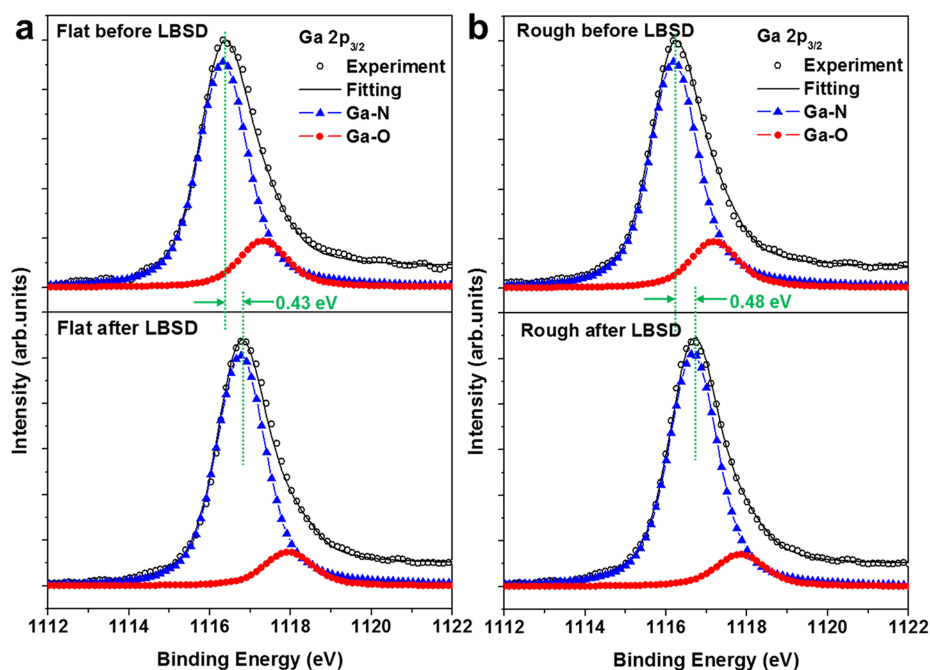

Figure 3. XPS spectra of the Ga $2p_{3/2}$ core levels measured from the metal/n-GaN interface regions: (a) flat before and after LBSD samples and (b) rough before and after LBSD samples. Vertical dashed lines indicate the peak positions of each core level. Open circles represent the experimental data.

the proposed LBSD on the ohmic-contact properties at the interface between the contact metal and the laser-based doped region in the n-GaN layers with flat and rough surface. Figure 2a shows the $I-V$ characteristics of the four types of n-GaN layers. It is observed that the flat and rough before LBSD samples exhibited quasi-ohmic behavior, whereas the flat and rough after LBSD samples exhibited perfect ohmic behavior. The specific contact resistance was calculated from the linear fitted line of a plot of the total resistance as a function of the contact-pad gap distance, as shown in Figure 2b. The results show that the average specific contact resistances of the flat before LBSD sample, rough before LBSD sample, flat after LBSD sample, and rough after LBSD sample were 1.47×10^{-4}, 3.42×10^{-4}, 1.56×10^{-5}, and 2.86×10^{-5} Ω cm^2, respectively. It should be considered that the specific contact resistance of the flat before LBSD sample is similar to that reported by other groups.[16,17] It is observed that the specific contact resistance of the rough before LBSD sample is slightly higher than that of the flat before LBSD sample. Moreover, the variations in the specific contact resistance data of the rough before LBSD sample are more prominent than those of other samples (see the Supporting Information, Figure S3) This worse ohmic behavior can be explained by the complex surface states of the n-GaN structures, such as the mixed crystal polarities of the N-polar (000−1) and semipolar (10−1−1) directions, impurities, and various defects (intrinsic, donorlike, and acceptor-like defects).[8,19] Another possible explanation is that the length of the lateral current transport path is not uniform owing to the rough and irregular surface between the contact pads.[20,21] On the other hand, it is interesting that the specific contact resistances significantly decreased after LBSD by more than 1 order of magnitude compared with those before LBSD. These results indicate that the LBSD technique is effective in improving the carrier transport from the metal contacts to the n-GaN layer regardless of the surface-state conditions. To explain the interdiffusion of Si atoms from a Si film to the n-GaN layer, quantification of Si-concentration depth profiles for the samples before and after LBSD was carried out using SIMS, as shown in Figure 2c. It was observed that the n-GaN before LBSD sample had a uniform Si dopant concentration of approximately 5×10^{18} cm^{-3}, whereas the Si dopant concentration of the n-GaN after LSBD sample gradually decreased from 5×10^{21} (near the top surface) to 5×10^{18} cm^{-3}. After LBSD, the Si interdiffusion length was approximately 1−1.5 μm; therefore, a highly doped layer with a doping level greater than 1×10^{20} cm^{-3} and a thickness of approximately 400 nm was formed near the top surface of the n-GaN layer.

To identify the possible mechanism for the improved nonalloyed ohmic characteristics of LBSD n-GaN, the chemical bonding states and surface binding energies at the metal/n-GaN interface were analyzed by XPS with a monochromatic aluminum Kα X-ray radiation source (a photon energy of 1486.6 eV). The binding energies of the measured spectra were corrected by means of a C 1s peak (284.6 eV). Figure 3 shows the XPS spectra of the Ga $2p_{3/2}$ core levels taken from the four types of n-GaN samples. The curves of the Ga $2p_{3/2}$ core levels were fitted by the mixed shape of Lorentzian and Gaussian curves with the modified Shirley-type background subtraction method to separate the energies of the peaks.[22] It is noted that the peaks of the Ga $2p_{3/2}$ core level consist of two peaks of Ga−N and Ga−O bonds after peak deconvolution. The spectra show that the peak position of the Ga $2p_{3/2}$ core level of the rough before LBSD sample is lower than that of the flat before LBSD sample by 0.13 eV. This negative shift in the binding energy means that the surface Fermi energy level (E_F) at the metal/n-GaN interface region moves closer to the valence band edge, which causes the upward movement of the interfacial band bending, thus increasing the effective Schottky barrier height (SBH) for electron injection and transport from the metal to the n-GaN surface and resulting in an increase in the specific contact resistance.[23] In general, it is believed that the

dx.doi.org/10.1021/am5031165 | ACS Appl. Mater. Interfaces 2014, 6, 16601−16609

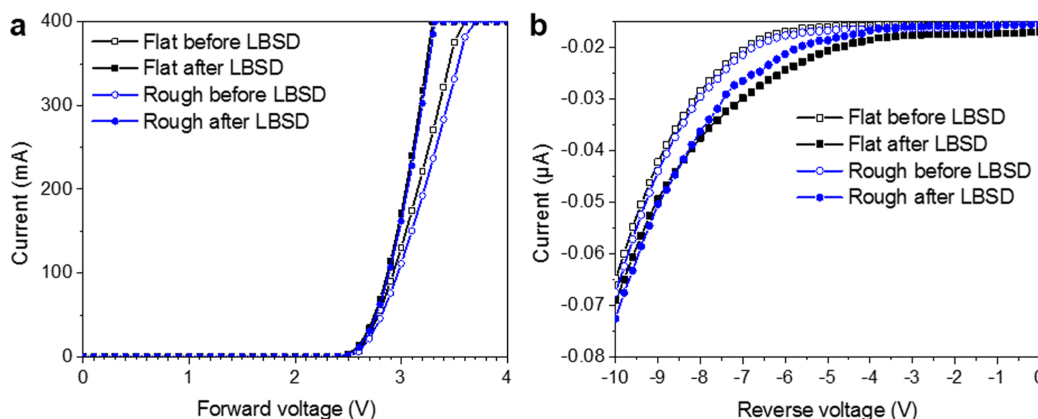

Figure 4. (a) Current versus forward voltage ($I-V$) characteristics and (b) reverse-leakage-current characteristics measured for the four types of TFLEDs.

movement of the surface E_F can be ascertained from the relative shift in the peak positions in the Ga-based core-level peaks.[24,25] After LBSD, the peak position of the Ga $2p_{3/2}$ core level is higher by 0.43 and 0.48 eV for the flat- and rough-surface samples, respectively, than that of the flat and rough before LBSD samples. These positive shifts in the binding energy indicate that the surface E_F at the metal/n-GaN interface region moves closer to the conduction band edge, which suppresses the upward movement of the interfacial band bending, thus dramatically decreasing the effective SBH for electron injection and transport from the metal to the n-GaN surface and resulting in improved ohmic contact properties and a decrease in the specific contact resistance.[26,27] These results are in good agreement with the measured data in Figure 2.

In addition, the relative N/Ga elemental ratio was investigated by comparing the peak areas of the N 1s and the Ga $2p_{3/2}$ (Ga−N) core levels. The calculated N/Ga ratios of the flat before LBSD sample, rough before LBSD sample, flat after LBSD sample, and rough after LBSD sample were found to be 1.0, 1.01, 0.71, and 0.73, respectively. Here, we note that the N/Ga ratio of the flat before LBSD sample is used as the reference with a normalized value of 1.0. A significant decrease in the N/Ga ratios was observed for both samples after LBSD. The small value of the N/Ga ratio implies that plenty of N-deficient regions were formed at the metal/n-GaN interface, which is attributed to the out-diffusion of N atoms (N vacancies, V_N) from the n-GaN layer. These results are comparable to the trends observed in other reports, which have demonstrated that a lower N/Ga ratio leads to the generation of N vacancies.[28,29] N vacancies located at a shallow energy level E_D of approximately 25 meV below the conduction band in GaN are well-known for acting as donors.[30] In the presence of Ga vacancies (V_{Ga}), the low N/Ga ratio may also be explained by the fact that the generation of N vacancies is more pronounced than that of Ga out-diffusion during the LBSD process.[31] Moreover, energetic Si atoms diffuse into the n-GaN lattice or subsurface at the same time when Si and n-GaN are irradiated by the KrF laser beam and are then easily incorporated into the GaN lattice, substituting for Ga on Ga sites in n-GaN (Si_{Ga}), because of their relatively lower formation energy.[32] The Si atoms at the Ga sites act as shallow donors in GaN that have a donor energy level E_D of approximately 22 or 30.8 meV below the conduction band and compensate for the acceptor-like Ga vacancies.[33,34] Thus, from above results, the generation of N vacancies, the substitution of Ga with Si, and the Si doping in GaN increase the electron concentration in the n-GaN subsurface, leading to the formation of highly doped thin n-GaN layers and resulting in a reduction in the potential barrier width at the metal/n-GaN interface. Therefore, the improved nonalloyed ohmic contacts after LBSD can be attributed to the combined effects of the reduced SBH, donor-like N vacancies, and Si doping. These effects provide a decrease in the effective SBH as well as the tunneling barrier width, which enhance the probability of electron tunneling across the metal/n-GaN interface. Considering these results, more detailed conceptual drawings associated with the mechanism of LBSD for the GaN lattice are presented in the Supporting Information, Figure S4.

To demonstrate the feasibility of the LBSD effects at the device level on the basis of the above unit-process results, flat- and rough-surface TFLEDs before and after LBSD were fabricated, and their performance was compared with each other. Figures 4a and 4b show a comparison of the $I-V$ and reverse-leakage-current characteristics measured from the four types of TFLEDs. In Figure 4a, the operating voltages of 3.45, 3.23, 3.53, and 3.25 V at 350 mA were measured for the flat before LBSD, flat after LBSD, rough before LBSD, and rough after LBSD TFLEDs, respectively. The corresponding series resistances extracted from the linear regions of the $I-V$ characteristics were 2.03, 1.3, 2.2, and 1.33 Ω for the flat before LBSD, flat after LBSD, rough before LBSD, and rough after LBSD TFLEDs, respectively. The lower series resistance is attributed to the formation of low-resistance n-type ohmic contacts, which could enhance the injection efficiency of the TFLEDs. On the other hand, it was found that a reduction in the operating voltage of 0.11 V was observed for the flat-surface TFLED before LBSD compared with the rough-surface TFLED before LBSD. The slightly higher operating voltage for the rough-surface TFLED before LBSD is caused by the relatively high contact resistance due to the undesirable effects of complex surface states, as mentioned earlier in the discussion of Figure 2. For both TFLEDs after LBSD, the flat and rough surfaces exhibit almost the same operating voltage. In particular, the reduced operating voltages of 0.22 and 0.28 V for the flat- and rough-surface TFLEDs after LBSD, as compared with those before LBSD, were observed because of the reduced contact resistance, decreased series resistance, and low sheet resistance of the thin highly doped n-GaN surface, which increase the injection efficiency and lateral current transport in the TFLED devices. The calculated sheet resistances were 66.3,

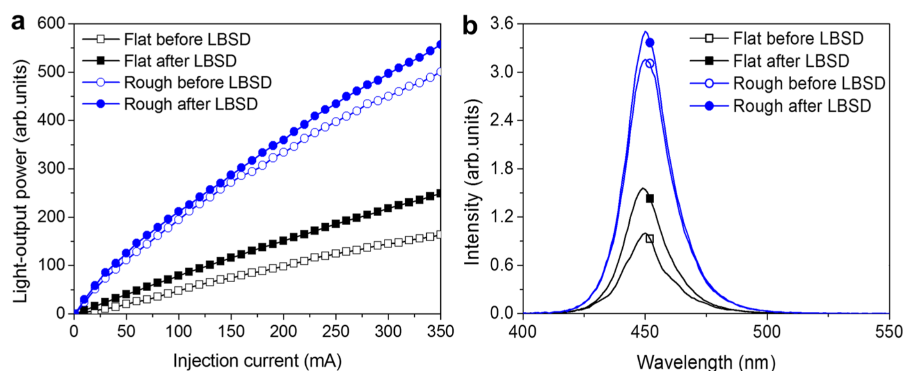

Figure 5. (a) Light-output power versus current ($L-I$) characteristics and (b) electroluminescence (EL) spectra measured for the four types of TFLEDs at an injection current of 350 mA.

40, 72, and 40.3 Ω/sq for the TFLEDs with the flat surface before LBSD, the flat surface after LBSD, the rough surface before LBSD, and the rough surface after LBSD, respectively. Moreover, the leakage-current characteristics of the four types of TFLEDs are shown in Figure 4b to identify the influence of LBSD on the device reliability. All TFLEDs exhibited similar leakage currents ranging from 64.8 to 72.6 nA at a reverse voltage of 10 V, which is sufficiently low to achieve highly efficient and reliable device performance. These results indicate that the use of LBSD does not affect the electrical characteristics of the LED devices.

Figure 5a shows the average light-output power versus the injection current for 20 LED chips randomly selected from each type of LED sample. The light-output power was measured using a calibrated large-area Si photodetector placed 1 cm from the top of the LED chip. With an injection current of 350 mA, the light-output power of the rough-surface TFLEDs before LBSD was increased by 204.8% compared with the flat-surface TFLEDs before LBSD, which is comparable to the enhancement in the light-output power reported previously.[4,6] This improved light-output power of the rough-surface TFLEDs before LBSD is due to the reduction in the total internal reflection at the GaN/air interface as well as random light-scattering effects from the roughened surface. It is also observed that the light-output powers at 350 mA for the flat- and rough-surface TFLEDs after LBSD are improved by 52.1 and 11.35%, respectively, compared to those for the flat- and rough-surface TFLEDs before LBSD. LBSD also reduces the chip-to-chip variation in the light-output power, thus enhancing the manufacturing yield and uniformity (see the Supporting Information, Figure S5). In addition, the largest electroluminescence (EL) intensity was observed from the rough-surface TFLEDs after LBSD, as seen in the room-temperature EL spectra measured for the four types of TFLEDs at 350 mA in Figure 5b. The dominant peaks in the EL spectra for the four types of TFLEDs were almost same and positioned at approximately 449 nm.

To confirm the effect of LBSD on the light-output enhancement and current distribution of the TFLEDs, n-GaN surface images obtained by AFM and the light intensity distribution at 20 mA were compared with each other, as shown in Figure 6. The surface morphologies of the rough-surface TFLEDs before and after LBSD exhibit hexagonal pyramidlike features randomly distributed with microscale or nanoscale patterns whose heights are in the range of 0.5−1.0 μm. It is observed that the root-mean-square roughness of the flat and rough surfaces before LBSD (after LBSD) is 4.21 nm (13.47 nm) and 255 nm (261.57 nm), respectively (Figures 6a−d). On the basis of these results, LBSD causes a slight increase in the surface roughness, leading to an increase in light extraction in the surface-emission area due to additional multiple light-scattering effects that results in a light-output enhancement. The enhancement rate in the light-output power and EL intensity for the flat-surface TFLEDs after LBSD is much larger than that in the rough-surface TFLEDs after LBSD. This is because the scattering effects due to the textured surface of the rough-surface TFLEDs might slightly diminish the increasing rate in light extraction according to LBSD effects. In Figure 6e, as predicted, the light-intensity distributions follow a similar trend as the light-output power. The light-intensity distributions of the TFLEDs after LBSD exhibited more uniform and strong light-output characteristics compared with those of TFLEDs before LBSD. In particular, the rough-surface TFLEDs after LBSD exhibited a uniform current distribution as well as the strongest light intensity. Considering all of the above results, these improvements are thought to be due to the combined effects of effective current injection, the uniform current distribution from the metal to the n-GaN layer because of its highly doped nature, and additional multiple light-scattering effects by LBSD, leading to more uniform and stronger light emission as well as lower operating voltages.

4. CONCLUSION

In summary, we demonstrated improved electrical and optical performance in TFLEDs by applying LBSD to the n-GaN surface. At a current of 350 mA, experimental results showed that the light-output powers of the flat- and rough-surface TFLEDs after LBSD were 52.1% and 11.35% higher than those before LBSD, respectively. The corresponding operating voltages were decreased by 0.22 and 0.28 V for the flat- and rough-surface TFLEDs after LBSD, respectively, because the specific contact resistances were significantly decreased to 1.56×10^{-5} and 2.86×10^{-5} Ω cm^2 for the flat- and rough-surface after LBSD samples, respectively. Furthermore, LBSD did not degrade the electrical properties of the TFLEDs, as evidenced by the low reverse-leakage currents. These results reveal that the proposed LBSD method is quite useful for enhancing the overall performance of the TFLEDs because of better current distribution, better current injection, and additional light-scattering effects in these devices.

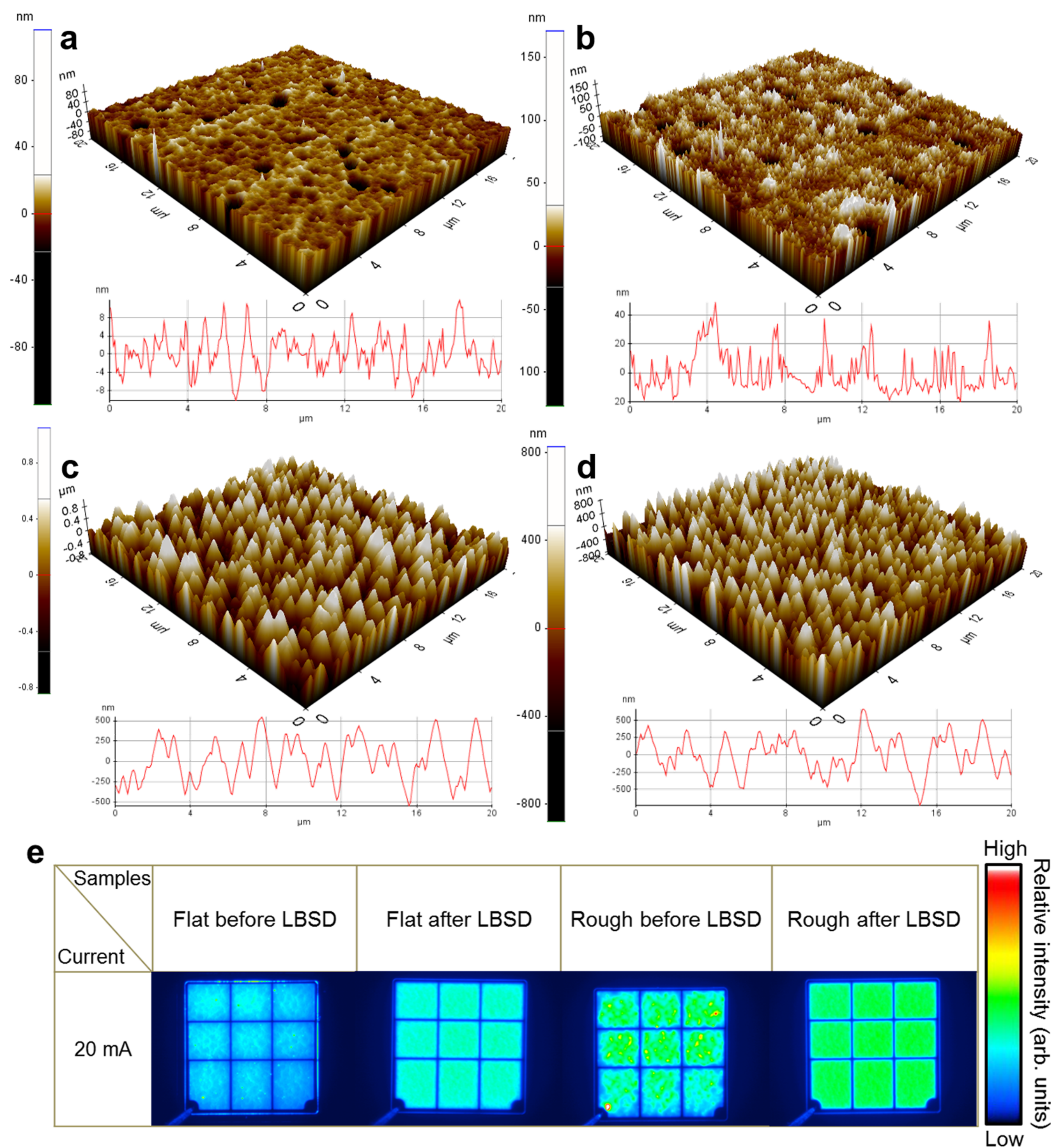

Figure 6. AFM surface images obtained from the flat-surface TFLEDs (a) before and (b) after LBSD and the rough-surface TFLEDs (c) before and (d) after LBSD. The image scale is 20 μm × 20 μm. The graphs below the AFM images show the height differences across a horizontal line on the surface. (e) Light-intensity distribution images of the four types of TFLEDs taken at injection currents of 20 mA for a clear comparison. The relative light intensities are indicated by the color bar located on the right-hand side of the light-intensity distribution images.

■ ASSOCIATED CONTENT

Ⓢ Supporting Information

Schematic of the fabrication process of the TFLED chip (Figure S1); a schematic of the laser-based Si doping system, a 2 in. wafer-level photograph including the magnified microscope images, and an emission photograph of the flat- and rough-surface TFLEDs before and after LBSD (Figure S2); the variations in the specific contact resistances of the four types of n-GaN samples (Figure S3); the conceptual drawings of the mechanism for the LBSD process (Figure S4); and the variation in the light-output power of the four types of TFLEDs (Figure S5). This material is available free of charge via the Internet at http://pubs.acs.org/.

dx.doi.org/10.1021/am5031165 | ACS Appl. Mater. Interfaces 2014, 6, 16601−16609

■ AUTHOR INFORMATION

Corresponding Author

*E-mail: tgkim1@korea.ac.kr. Phone: +82-2-3290-3255. Fax: +82-2-924-5119.

Notes

The authors declare no competing financial interest.

■ ACKNOWLEDGMENTS

This work was supported by a National Research Foundation of Korea (NRF) grant funded by the Korean Government (2011-0028769).

■ REFERENCES

(1) Pimputkar, S.; Speck, J. S.; DenBaars, S. P.; Nakamura, S. Prospects for LED Lighting. *Nat. Photonics* **2009**, *3*, 180−182.
(2) Tan, S. T.; Sun, X. W.; Demir, H. V.; DenBaars, S. P. Advances in the LED Materials and Architectures for Energy-Saving Solid-State Lighting Toward "Lighting Revolution. *IEEE Photonics J.* **2012**, *4*, 613−619.
(3) DenBaars, S. P.; Feezell, D.; Kelchner, K.; Pimputkar, S.; Pan, C.-C.; Yen, C.-C.; Tanaka, S.; Zhao, Y.; Pfaff, N.; Farrell, R.; Iza, M.; Keller, S.; Mishra, U.; Speck, J. S.; Nakamura, S. Development of Gallium-Nitride-Based Light-Emitting Diodes (LEDs) and Laser Diodes for Energy-Efficient Lighting and Displays. *Acta Mater.* **2013**, *61*, 945−951.
(4) Lin, C.-H.; Tu, C.-G.; Chen, H.-S.; Hsieh, C.; Chen, C.-Y.; Liao, C.-H.; Kiang, Y.-W.; Yang, C. C. Vertical Light-Emitting Diodes with Surface Gratings and Rough Surfaces for Effective Light Extraction. *Opt. Express* **2013**, *21*, 17686−17694.
(5) Chuang, S.-H.; Pan, C.-T.; Shen, K.-C.; Ou, S.-L.; Wuu, D.-S.; Horng, R.-H. Thin Film GaN LEDs Using a Patterned Oxide Sacrificial Layer by Chemical Lift-Off Process. *IEEE Photonics Technol. Lett.* **2013**, *25*, 2435−2438.
(6) Fujii, T.; Gao, Y.; Sharma, R.; Hu, E. L.; DenBaars, S. P.; Nakamura, S. Increase in the Extraction Efficiency of GaN-Based Light-Emitting Diodes via Surface Roughening. *Appl. Phys. Lett.* **2004**, *84*, 855.
(7) Tian, P.; Chen, Z.; Sun, Y.; Qi, S.; Zhang, H.; Deng, J.; Yu, F.; Yu, T.; Kang, X.; Qin, Z.; Zhang, G. Phase Distribution in Eutectic AuSn Layer Changed by Temperature Ramping Rate and Its Effect on the Performance of GaN-Based Vertical Structure LEDs. *Mater. Sci. Eng., B* **2010**, *175*, 213−216.
(8) Kim, H.; Ryou, J.-H.; Dupuis, R. D.; Lee, S.-N.; Park, Y.; Jeon, J.-W.; Seong, T.-Y. Electrical Characteristics of Contacts to Thin Film N-Polar n-Type GaN. *Appl. Phys. Lett.* **2008**, *93*, 192106.
(9) Yan, L.-J.; Kuo, C. H.; Sheu, J.-K.; Lee, M.-L.; Tseng, W.-C. Non-Alloyed Cr/Au Ohmic Contacts to N-Face and Ga-Face n-GaN. *J. Alloys Compd.* **2012**, *516*, 38−40.
(10) Jeon, J.-W.; Seong, T.-Y.; Kim, H.; Kim, K.-K. TiN/Al Ohmic Contacts to N-Face n-Type GaN for High-Performance Vertical Light-Emitting Diodes. *Appl. Phys. Lett.* **2009**, *94*, 042102.
(11) Liu, L.; Ling, M.; Yang, J.; Xiong, W.; Jia, W.; Wang, G. Efficiency Degradation Behaviors of Current/Thermal Co-Stressed GaN-Based Blue Light Emitting Diodes with Vertical-Structure. *J. Appl. Phys.* **2012**, *111*, 093110.
(12) Li, C.-K.; Wu, Y.-R. Study on the Current Spreading Effect and Light Extraction Enhancement of Vertical GaN/InGaN LEDs. *IEEE Trans. Electron Devices* **2012**, *59*, 400−407.
(13) Tu, S. H.; Chen, J. C.; Hwu, F. S.; Sheu, G. J.; Lin, F. L.; Kuo, S. Y.; Chang, J. Y.; Lee, C. C. Characteristics of Current Distribution by Designed Electrode Patterns for High Power ThinGaN LED. *Solid-State Electron.* **2010**, *54*, 1438−1443.
(14) Kim, D. W.; Lee, H. Y.; Yoo, M. C.; Yeom, G. Y. Highly Efficient Vertical Laser-Liftoff GaN-Based Light-Emitting Diodes Formed by Optimization of the Cathode Structure. *Appl. Phys. Lett.* **2005**, *86*, 052108.
(15) Lee, W.-C.; Wang, S.-J.; Wang, P.-R.; Uang, K.-M.; Chen, T.-M.; Kuo, D.-M.; Wang, P.-H. Enhanced Performance of GaN-Based Vertical Light-Emitting Diodes with Circular Protrusions Surmounted by Hexagonal Cones and Indium−Zinc Oxide Current Spreading Layer. *Appl. Phys. Express* **2011**, *4*, 072104.
(16) Wang, L.; Zhang, Y.; Li, X.; Liu, Z.; Guo, E.; Yi, X.; Wang, J.; Zhu, H.; Wang, G. Partially Sandwiched Graphene as Transparent Conductive Layer for InGaN-Based Vertical Light Emitting Diodes. *Appl. Phys. Lett.* **2012**, *101*, 061102.
(17) Ueda, T.; Ishida, M.; Yuri, M. Separation of Thin GaN from Sapphire by Laser Lift-Off Technique. *Jpn. J. Appl. Phys.* **2011**, *50*, 041001.
(18) Jakiela, R.; Barcz, A.; Dumiszewska, E.; Jagoda, A. Si Diffusion in Epitaxial GaN. *Phys. Status Solidi C* **2006**, *3*, 1416−1419.
(19) Jung, Y.; Baik, K. H.; Ren, F.; Pearton, S. J.; Kim, J. Effects of Photoelectrochemical Etching of N-Polar and Ga-Polar Gallium Nitride on Sapphire Substrates. *J. Electrochem. Soc.* **2010**, *157*, H676−H678.
(20) Redaelli, L.; Muhin, A.; Einfeldt, S.; Wolter, P.; Weixelbaum, L.; Kneissl, M. Ohmic Contacts on N-Face n-Type GaN After Low Temperature Annealing. *IEEE Photon. Technol. Lett.* **2013**, *25*, 1278−1281.
(21) Gong, R.; Wang, J.; Liu, S.; Dong, Z.; Yu, M.; Wen, C. P.; Cai, Y.; Zhang, B. Analysis of Surface Roughness in Ti/Al/Ni/Au Ohmic Contact to AlGaN/GaN High Electron Mobility Transistors. *Appl. Phys. Lett.* **2010**, *97*, 062115.
(22) Shi, K.; Liu, X. L.; Li, D. B.; Wang, J.; Song, H. P.; Xu, X. Q.; Wei, H. Y.; Jiao, C. M.; Yang, S. Y.; Song, H.; Zhu, Q. S.; Wang, Z. G. Valence Band Offset of GaN/Diamond Heterojunction Measured by X-Ray Photoelectron Spectroscopy. *Appl. Surf. Sci.* **2011**, *257*, 8110−8112.
(23) Reddy, N. N. K.; Reddy, V. R.; Choi, C.-J. Influence of Rapid Thermal Annealing Effect on Electrical and Structural Properties of Pd/Ru Schottky Contacts to n-Type GaN. *Mater. Chem. Phys.* **2011**, *130*, 1000−1006.
(24) Sun, J.; Rickert, K. A.; Redwing, J. M.; Ellis, A. B.; Himpsel, F. J.; Kuech, T. F. p-GaN Surface Treatments for Metal Contacts. *Appl. Phys. Lett.* **2000**, *76*, 415.
(25) Reddy, V. R.; Ravinandan, M.; Rao, P. K.; Choi, C.-J. Effects of Thermal Annealing on the Electrical and Structural Properties of Pt/Mo Schottky Contacts on n-Type GaN. *J. Mater. Sci.: Mater. Electron.* **2009**, *20*, 1018−1025.
(26) Jang, H. W.; Lee, J.-H.; Lee, J.-L. Characterization of Band Bendings on Ga-Face and N-Face GaN Films Grown by Metalorganic Chemical-Vapor Deposition. *Appl. Phys. Lett.* **2002**, *80*, 3955.
(27) Hou, W.; Detchprohm, T.; Wetzel, C. Effects of Oxygen Thermal Annealing Treatment on Formation of Ohmic Contacts to n-GaN. *Appl. Phys. Lett.* **2012**, *101*, 242105.
(28) Kawakami, R.; Niibe, M.; Nakano, Y.; Konishi, M.; Mori, Y.; Takeichi, A.; Tominaga, K.; Mukai, T. Comparison Between Damage Characteristics of p-and n-GaN Surfaces Etched by Capacitively Coupled Radio Frequency Argon Plasmas. *Jpn. J. Appl. Phys.* **2013**, *52*, 05EC05.
(29) Zhang, W.; Zhang, J.; Wu, Z.; Chen, S.; Li, Y.; Tian, Y.; Dai, J.; Chen, C.; Fang, Y. Improved Ohmic Contacts to Plasma Etched n-$Al_{0.5}Ga_{0.5}N$ by Annealing Under Nitrogen Ambient Before Metal Deposition. *J. Appl. Phys.* **2013**, *113*, 094503.
(30) Yang, Q.; Feick, H.; Weber, E. R. Observation of a Hydrogenic Donor in the Luminescence of Electron-Irradiated GaN. *Appl. Phys. Lett.* **2003**, *82*, 3002−3004.
(31) Jang, H. W.; Kim, J. K.; Lee, J. L.; Schroeder, J.; Sands, T. Electrical Properties of Metal Contacts on Laser-Irradiated n-Type GaN. *Appl. Phys. Lett.* **2003**, *82*, 580−582.
(32) Boguslawski, P.; Bernholc, J. Doping Properties of C, Si, and Ge Impurities in GaN and AlN. *Phys. Rev. B* **1997**, *56*, 9496−9505.
(33) Götz1, W.; Johnson, N. M.; Chen, C.; Liu, H.; Kuo, C.; Imler, W. Activation Energies of Si Donors in GaN. *Appl. Phys. Lett.* **1996**, *68*, 3144.

(34) Wang, H.; Chen, A.-B. Calculation of Shallow Donor Levels in GaN. *J. Appl. Phys.* **2000**, *87*, 7859.